Sensors and Actuators B 252 (2017) 706–711

Contents lists available at ScienceDirect

Sensors and Actuators B: Chemical

journal homepage: www.elsevier.com/locate/snb

Electrostatics-driven sensing platform: Graphene oxide-probe conjugate for the selective detection of pyrophosphate

Dong-Nam Lee, Jungwon Kim, Jae Gyu Jang, Jong-In Hong*

Department of Chemistry, College of Natural Sciences, Seoul National University, Seoul 08826, Republic of Korea

ARTICLE INFO

Article history:
Received 30 December 2016
Received in revised form 26 May 2017
Accepted 4 June 2017
Available online 10 June 2017

Keywords:
Electrostatic interaction
Fluorescent probe
Graphene oxide
Pyrophosphate
Polymerase chain reaction monitoring

ABSTRACT

The development of a pyrophosphate (PPi) detection method has been challenging because PPi is a natural concomitant of many enzymatic reactions. The key issue of developing chemosensors for PPi is the discrimination of PPi from excess nucleoside triphosphates (NTPs). Herein, we report a new PPi detection method modulating electrostatic interactions between a negatively charged graphene oxide (GO) and a positively charged synthetic probe **1** before and after PPi recognition. The combination of probe **1** and GO resulted in excellent selectivity towards PPi even in excess adenosine triphosphate (ATP). Consequently, this sensing system was successfully applied to real-time monitoring of a DNA polymerase chain reaction (PCR).

1. Introduction

The development of a pyrophosphate (PPi) detection method with high selectivity and sensitivity has been challenging in the post-genomic era because PPi is a natural concomitant of gene replication and expression catalyzed by DNA/RNA polymerases [1] and aminoacyl-tRNA synthetases [2,3], respectively. These enzymatic activities are linked to common genetic diseases; therefore, their monitoring is now indispensable in therapeutic and diagnostic research [4–6]. While traditional methods such as gel electrophoresis [7] and scintillation counting [8,9] can be used, a fluorescent detection method is still desired because of its usefulness in high-throughput screening [10,11]. For decades, phenoxo-bridged binuclear Zn^{2+}–dipicolylamine complex (bisZnDPA) has been extensively utilized as a receptor unit (ligand) for the detection of PPi [12–21]. However, its low selectivity for PPi in the presence of excess nucleoside triphosphates (NTPs) remains a major obstacle to the real-time monitoring of enzymatic reactions involving the release of PPi, as a small amount of PPi is typically released in the presence of a large amount of NTPs during the enzymatic reactions. To address this issue, we developed a new PPi detection method that combines the well-known surface characteristics of graphene oxide (GO) and selective recognition ability of bisZnDPA-based probes.

GO has gained widespread attention as a fluorescent sensing platform for detecting DNA, metal ions, and many other entities, because of its remarkable water-solubility, biocompatibility, and fluorescence quenching ability [22]. GO bears an aromatic domain and is negatively charged under physiological conditions, and therefore, complex interplay exists between π-π stacking/hydrophobic interactions and electrostatic interactions, both with aromatic species (e.g. nucleobase of NTPs and aromatic side chain of amino acids) [23–26] and positively charged molecules [27–29] to form an energy- or charge-transfer complex. Thus, a probe consisting of an aromatic moiety-containing fluorophore and positively charged ligand would be useful for developing a conjugate system with GO. In addition, cooperation of the selective recognition ability of the bisZnDPA ligand and versatile features of GO may be promising for discriminating PPi from NTPs; the bisZnDPA-based probe exhibits fluorescence responses depending on the PPi (or NTP) concentration, while GO interrupts the binding of sterically bulky NTPs to the bisZnDPA bound on the surface of GO [23–26]. In this regard, a positively-charged probe **1** (6,8-bis(zinc^{2+}-dipicolylamine)-7-hydroxy-3-*p*-tolyl-coumarin) in which the bisZnDPA is directly linked to a coumarin fluorophore was designed to develop a conjugate system (GO-**1**) on the surface of GO based on electrostatic attraction (Scheme 1).

The sensing concept is guided by modulation of the electrostatic interactions between GO and probe **1** before and after PPi recognition. The fluorescence of **1** was markedly enhanced when PPi was added to the electrostatically attractive patch (GO-**1**), which originates from *charge inversion* in **1**-PPi upon binding PPi, con-

* Corresponding author.
E-mail address: jihong@snu.ac.kr (J.-I. Hong).

http://dx.doi.org/10.1016/j.snb.2017.06.018
0925-4005/

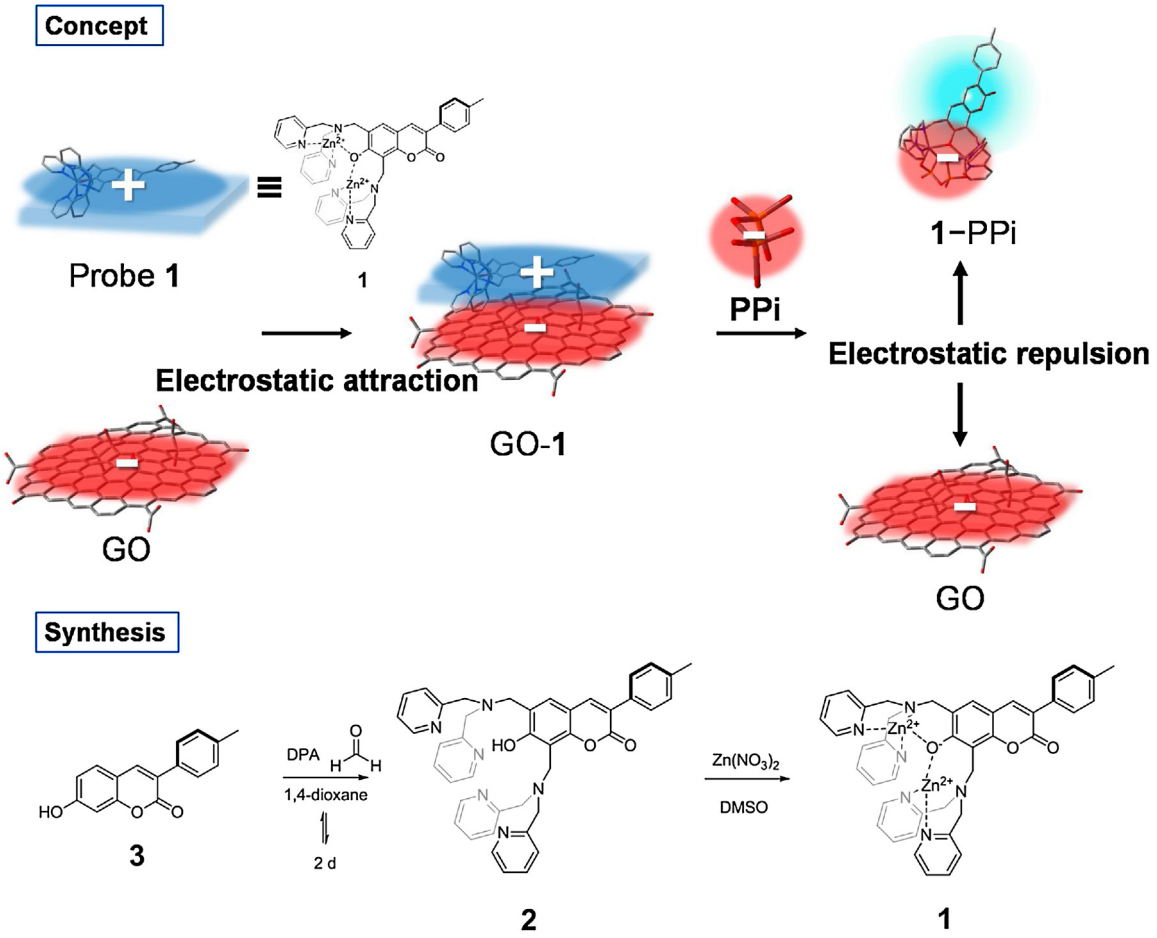

Scheme 1. Schematic representation of the PPi detection mechanism and synthetic scheme of probe **1**.

comitantly resulting in Coulombic repulsion between GO and **1**-PPi (Scheme 1). Additionally, ionic strength modulation of a solution caused subtle changes in sensitivity and increased the PPi selectivity over ATP. Consequently, this concept was successfully applied in real-time monitoring of DNA polymerase chain reaction (PCR) that requires highly selective detection of PPi released during PCR.

2. Experimental section

2.1. Synthetic procedures

2.1.1. Synthesis of *2*

Compound **3** was prepared following the literature method [30]. To a solution of 37% aqueous formaldehyde solution (2.53 mL, 30 mmol) in 1,4-dioxane (60 mL) was added bis(2-pyridylmethyl)amine (5.4 mL, 30 mmol), and the reaction mixture was stirred at 50 °C for 5 h. Then, compound **3** (2.9 g, 11.5 mmol) was added to the reaction mixture. The resulting reaction mixture was stirred at 110 °C for 2 days, cooled down to room temperature (RT, 25 °C), and concentrated under reduced pressure using a rotary evaporator. The crude product was purified by flash column chromatography using CH_3OH:CH_2Cl_2 (gradient eluent, from 0:100 to 3:100) to give compound **2** (yellow crumbly solid) in 65% yield. ^{1}H NMR (DMSO-d_6, 300 MHz): δ 12.79 (br, 1H), 8.51 (d, 2H, J = 4.2 Hz), 8.48 (d, 2H, J = 4.5 Hz), 8.11 (s, 1H), 7.75–7.61 (m, 7H), 7.56–7.49 (m, 4H), 7.27–7.22 (m, 6H), 4.01 (s, 2H), 3.88 (s, 4H), 3.82 (s, 4H), 3.77 (s, 2H), 2.35 (s, 3H); ^{13}C NMR ($CDCl_3$, 75 MHz): δ 161.1, 160.4, 159.3, 158.7, 152.8, 148.9, 148.7, 140.4, 138.0, 136.8, 136.6, 132.5, 129.1, 128.4, 128.3, 123.3, 123.2, 123.2, 122.8, 122.1, 122.1, 111.7, 110.5, 59.9, 59.9, 53.5, 47.6, 21.3; HRMS (FAB$^+$, m-NBA): $[M+H]^+$ calculated for $C_{42}H_{39}N_6O_3$ 675.3084, observed 675.3078.

2.1.2. Synthesis of *1*

To a solution of **2** in DMSO (10 mM, 0.5 mL) was added 0.5 mL of 20 mM $Zn(NO_3)_2{\cdot}6H_2O$ stock solution in DMSO. After aging for 30 min at RT, the resulting solution was used as a stock solution of **1** (5 mM) without further purification (greenish solution, quantitative yield) [31]. ^{1}H NMR (DMSO-d_6, 300 MHz): δ 8.54 (br, 4H), 7.98 (d, 4H, J = 6.6 Hz), 7.84 (s, 1H), 7.60–7.52 (m, 6H), 7.40 (br, 4H), 7.25 (d, 2H, J = 8.1 Hz), 7.19 (s, 1H), 4.39–4.09 (m, 8H), 3.84 (s, 2H), 3.72 (s, 2H), 2.33 (s, 3H); HRMS (FAB$^+$, m-NBA): $[M+2NO_3^-]^+$ calculated for $C_{42}H_{37}N_8O_9Zn_2$ 925.1266, observed 925.1264.

2.2. Preparation of GO-*1* solution and spectroscopic measurements

GO sheet was purchased from Angstron Materials (Graphene oxide N002-PS). A stock solution of GO (0.1 wt%) was obtained by sonicating the GO solution for 2 h in EtOH:H_2O (1:1) solution. A mixture of GO and probe **1** was obtained by the addition of 100 μL of the GO stock solution (0.1 wt%) to 10 mL of probe **1** solution (1 μM in HEPES buffer, pH 7.4, HEPES = 2-[4-(2-hydroxy-ethyl)-1-piperazinyl]ethanesulfonic acid), and the resulting mixture was shaken for 5 min to make a homogeneous solution. Then, the mixture was centrifuged at 4000 rpm for 30 min. The resulting supernatants were collected, and aged for 2 days at RT to make a thermodynamically stable form of GO-**1**. Each analyte was added

to the GO-**1** solution, and the fluorescence intensity was measured with excitation at 367 nm (slit width: 5 × 3 nm, sensitivity: high).

2.3. Atomic force microscopy (AFM), X-ray photoelectron spectroscopy (XPS), Raman spectroscopy, and Fourier transform infrared (FTIR) spectroscopy, and X-ray diffraction (XRD) spectroscopy

AFM images were acquired in non-contact mode at a scan rate of 1 Hz under ambient atmosphere using a Veeco NanoScope IV instrument. Samples for AFM experiments were prepared by a simple drop-casting method: the solutions (GO, probe **1**) were deposited onto silicon wafer, washed carefully 3 times with deionized water, and allowed to dry in air. XPS experiments were carried out using a Kratos Axis-HIS instrument (anode material: Mg in Mg/Al dual anode, X-ray power: 15 mA & 12 kV). Raman spectroscopy was carried out using a Horiba LabRAM HR Evolution spectrometer (λ = 532 nm). The FTIR spectra were obtained by a Thermo Scientific Nicolet 6700 (USA) spectrometer in a range of 500–4000 cm^{-1}. X-ray diffraction (XRD) was taken on a Bruker D8 ADVANCE with DAVINCI (Detector: LYNXEYE XE, Generator: 40 kV & 40 mA). Samples for XPS, Raman, FTIR, and XRD experiments were prepared by the same procedure used for AFM experiments.

2.4. Polymerase chain reaction (PCR) monitoring

The primers of *C2-EGFP* (Forward primer: 5′-GAACAAGGATCCGTGAGCAAGGGCGAGGAGCT-3′; Reverse primer: 5′-CCGTAACTCGAGCGGTACAGCTCGTGCATGGC-3′) were purchased from MACROGEN. PCR was performed with the following components in a PCR microcentrifuge tube: Lyophilized HS Taq PCR Master Mix (TaKaRa), 0.2 μM final concentration of each primer, 100 ng of template DNA, and 23 μL of nuclease-free water. The thermal cycling program with Mastercycler started at 95 °C for 2 m, then 30 s denaturation at 95 °C, 45 s annealing at 55 °C, 55 s elongation at 72 °C and a final elongation at 72 °C for another 5 m. The PCR was repeated for 10–15 cycles. After PCR, the reaction mixture was cooled down to RT. The PCR product (2–10 μL per each cycle) was added into 1 mL of GO-**1** solution in 10 mM HEPES buffer. The fluorescence change was measured at 470 nm and gel electrophoresis of PCR products was carried out on 1% agarose gel to compare the existence of amplified DNA bands and the corresponding fluorescence changes. The amplified DNA on gel electrophoresis was stained by ethidium bromide (20 μg/tube). The DNA band image was then imported into the Adobe Photoshop CS6 software to digitize the changes in fluorescence, and the mean fluorescence intensity was determined from the image histogram.

3. Results and discussion

3.1. Synthesis of probe *1*

The bisZnDPA complex of probe **1** was easily introduced in two simple steps: the Mannich reaction of a coumarin derivative (**3**) with bis(2-pyridylmethyl)amine in the presence of formaldehyde afforded **2**, which was treated with an aqueous solution of $Zn(NO_3)_2$ (2 equiv.) to produce dinuclear Zn^{2+}-complex (probe **1**) (Scheme 1). The geometry optimized structure of probe **1** by the density functional theory (DFT) calculation is shown in Fig. S1.

3.2. Confirmation of the GO-*1* formation

The GO sheet was characterized as shown in Fig. S2. The Raman spectrum shows two prominent peaks at ~1350 cm^{-1} (D band) and ~1590 cm^{-1} (G band) that come from the defect of the sp^2 carbons and the bond stretching motion of sp^2 hybridized carbon atoms, respectively [32]. The XRD spectrum shows (001) diffraction peak at $2\theta = 10.1°$, which indicates a large interlayer distance (~0.8 nm) attributed to the presence of oxygen-containing functional groups (hydroxyl, epoxy, and carboxyl groups) [33]. The functional groups on the GO sheet were also identified by the FTIR spectrum: the broad and intense absorption band around 3400 cm^{-1} due to O—H stretching vibrations, the band at 1724 cm^{-1} due to carboxylic C=O stretching vibrations, the band at 1619 cm^{-1} due to sp^2 C=C vibrations, the band at 1391 cm^{-1} due to epoxy C—O vibrations, and the band at 1036 cm^{-1} due to alkoxy C—O vibrations [34].

The GO sheet and probe **1** were mixed (GO: 0.001 wt%, probe **1**: 1 μM in 10 mM HEPES buffer) together to produce GO-**1**. Strong interplay between GO and **1** was monitored by spectroscopic changes in **1**; GO-**1** showed a slightly broadened absorption band compared to coumarin absorption (probe **1**) because of the aromatic stacking of GO and **1** (Fig. 1a) [27]. The fluorescence of **1** was completely quenched because of strong photo-induced electron or energy transfer between **1** and GO upon adsorption of probe **1** to GO (Fig. 1b) [23–29]. X-ray photoelectron spectroscopy (XPS) was employed to confirm the adsorption of probe **1** onto the GO sheet. The XPS of GO-**1** exhibited two detectable peaks of Zn2p centered at 1020.6 and 1043.6 eV, originating from probe **1**, while GO itself showed no detectable signals [35]. After treatment with a PPi solution (10 μM), the corresponding peaks disappeared because of the expulsion of bound probe **1** from GO (Fig. S3). Atomic force microscopy (AFM) images showed that the thickness of the GO sheet was 1.8 nm, which is similar to that reported previously [36]. In comparison, the average thickness of GO-**1** was determined to be 2.3 nm (Fig. S4), indicating that GO was covered with probe **1** [37]. Raman spectra revealed that the G band of GO shifted to lower frequencies (from 1597 cm^{-1} to 1588 cm^{-1}) upon the addition of probe **1** compared to that of GO alone (Fig. S5), which indicates that probe **1** was adsorbed onto GO [38]. Therefore, XPS, AFM, and Raman data confirmed the formation of GO-**1**.

3.3. Photophysical property of GO-*1*

The spectral behavior of GO-**1** toward PPi was investigated in 10 mM HEPES buffer using fluorescence spectroscopy [39]. When increasing amounts of PPi were added to GO-**1**, the fluorescence of **1** was gradually increased at an λ_{max} of 470 nm, which is attributed to the probe desorption from GO in the form of **1**-PPi as a result of the reversal of electrostatic forces (Fig. 1c); electrostatic attractive forces between GO and probe **1** were changed to electrostatic repulsive forces between GO and **1**-PPi upon addition of PPi to the GO-**1** conjugate. Furthermore, an outstanding sensitivity of GO-**1** toward PPi (detection limit of 6.5×10^{-8} M and quantification limit of 2.0×10^{-7} M) was obtained with a linear dynamic range of 0–2 μM (Fig. S6). GO-**1** also showed a large ON/OFF ratio ($\Delta F = 3.9 \times 10^2$) upon addition of 8 μM PPi (Fig. S11e), which is much larger than the value obtained from the addition of PPi to probe **1** ($\Delta F = 1.5$, quenching process) (Fig. S7). These results indicate that the GO-probe conjugate system is superior to the probe-only system with respect to the sensitivity towards PPi by the quenching effect of GO.

There was no significant change in the fluorescence intensity of GO-**1** upon treatment with other anions (8 μM) such as acetate (OAc^-), N_3^-, Cl^-, CO_3^{2-}, citrate, and more importantly, inorganic phosphate (Pi), AMP, ADP, and NTPs (ATP, GTP, CTP, TTP, UTP) (Fig. 1d). Also, the corresponding fluorescence changes were detected by naked eye (Fig. S8). Competitive selectivity studies further demonstrated a highly selective response of GO-**1** for PPi (Fig. S9). Other GO-probe conjugates formed with control probes, *i.e.*, a mononuclear Zn^{2+} complex (GO-**4**), non Zn^{2+}-coordinated compound (GO-**2**), and coumarin molecule without the bisZnDPA ligand (GO-**3**), exhibited essentially no fluorescence response to PPi addition (Chart S1 and Fig. S10). This demonstrates that the com-

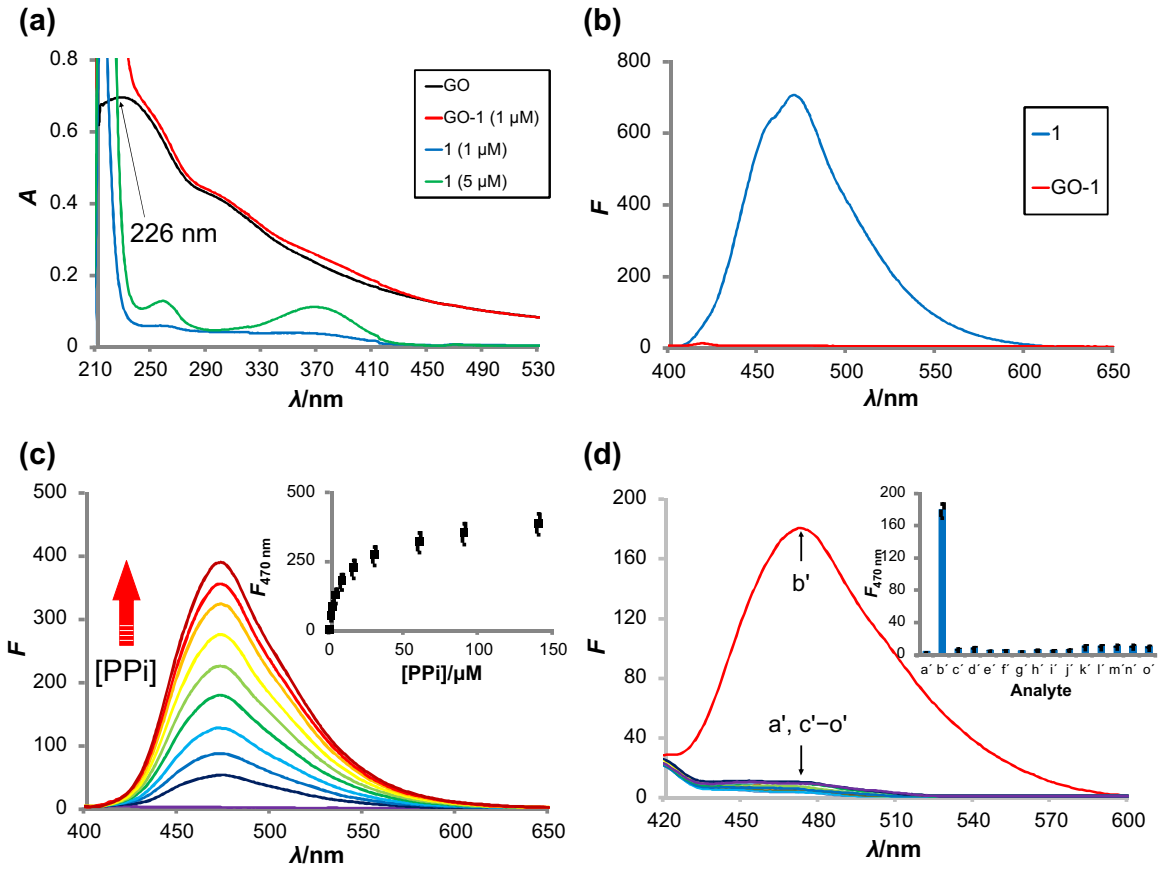

Fig. 1. (a) UV–vis. spectra of **1** (green line: 1 μM, blue line: 5 μM), GO (black line), and GO + probe **1** (red line) in 10 mM HEPES buffer (pH 7.4). (b) Fluorescence spectra of **1** (1 μM) before (blue line) and after GO addition (0.001 wt%, red line). (c) Fluorescence spectra of GO-**1** solution against concentration of PPi in 10 mM HEPES buffer (pH 7.4). The inset shows the fluorescence intensity changes at 470 nm upon addition of PPi. (d) Fluorescence spectra of GO-**1** solution in the presence of various anions ([all analytes] = 8 μM) such as (a') control (GO-**1**), (b') PPi, (c') OAc^-, (d') N_3^-, (e') Cl^-, (f') CO_3^{2-}, (g') citrate, (h') Pi, (i') AMP, (j') ADP, (k') ATP, (l') GTP, (m') CTP, (n') TTP, (o') UTP. The inset is a bar diagram showing fluorescence intensity of GO-**1** at 470 nm. The excitation wavelength was 367 nm. (For interpretation of the references to colour in this figure legend, the reader is referred to the web version of this article.)

plementary binding of PPi to the bisZnDPA ligand is integral in the sensing mechanism.

3.4. Ionic strength screening

Electrostatic interactions are influenced by the ionic strength of the medium, which was controlled by the concentration of HEPES (Fig. S11) [40]. The effect of ionic strength on the binding of PPi and ATP was systematically investigated. PPi was most effectively distinguished from ATP under the lowest ionic strength condition (Fig. 2a). Under low ionic strength conditions, the charges on both GO and **1** were relatively less screened by counter ions in the medium, leading to stronger Coulombic attractions between GO and probe **1** [40]. This resulted in more compact adsorption of probe **1** onto GO, where the bisZnDPA ligand of probe **1** may be covered with the oxygen-containing functional groups on the GO sheets compared to under higher ionic strength conditions. This may limit the approach of bulky NTPs into the ligand. However, smaller PPi molecules would be less influenced by the crowded ligand binding site. This may explain the discrimination of PPi from NTPs by GO-**1** under lower ionic strength conditions.

As the concentration of ions (I_{NaCl} = 0–100 mM, in 10 mM HEPES buffer) increased, the charges on both GO and **1** were increasingly screened by surrounding ions, leading to decreased Coulombic attraction between GO and probe **1** [40] and the gradual recovery of fluorescence of **1** (Fig. S12) [41].

3.5. PPi titration in excess ATP

Since there are many enzymatic reactions in which PPi is released in the presence of ATP, it is crucial to validate the selectivity of the sensing method that can distinguish PPi in the presence of excess amount of ATP. PPi titration experiments were performed in the presence of excess ATP (140 μM) (Fig. 2b and S13). Upon addition of ATP, the background signal of GO-**1** was slightly increased. However, subsequent addition of PPi (0.1–16 μM) into the ATP-containing solution led to a further noticeable increase in the fluorescence intensity with a micromolar detection limit. The best detection limit of 2.1×10^{-6} M was obtained in the lowest ionic strength solution (1 mM HEPES buffer) (Fig. 2b) among the buffer solutions tested. As indicated above, a decreasing ionic strength of the medium resulted in a decreased background fluorescence signal in the presence of excess ATP, while also increasing the ON/OFF ratio upon subsequent PPi titration. Our findings demonstrate that GO-**1** is a selective and sensitive sensor for the detection of PPi even in the presence of excess ATP, which gives substantial improvement over other sensing methods (Table S1).

3.6. PCR monitoring

Finally, we successfully applied the GO-**1** conjugate for fluorescence monitoring of PCR, which requires a highly sensitive and selective response for PPi over dNTPs. The band intensity on gel electrophoresis reveals the degree of DNA extension (Fig. 2c), which

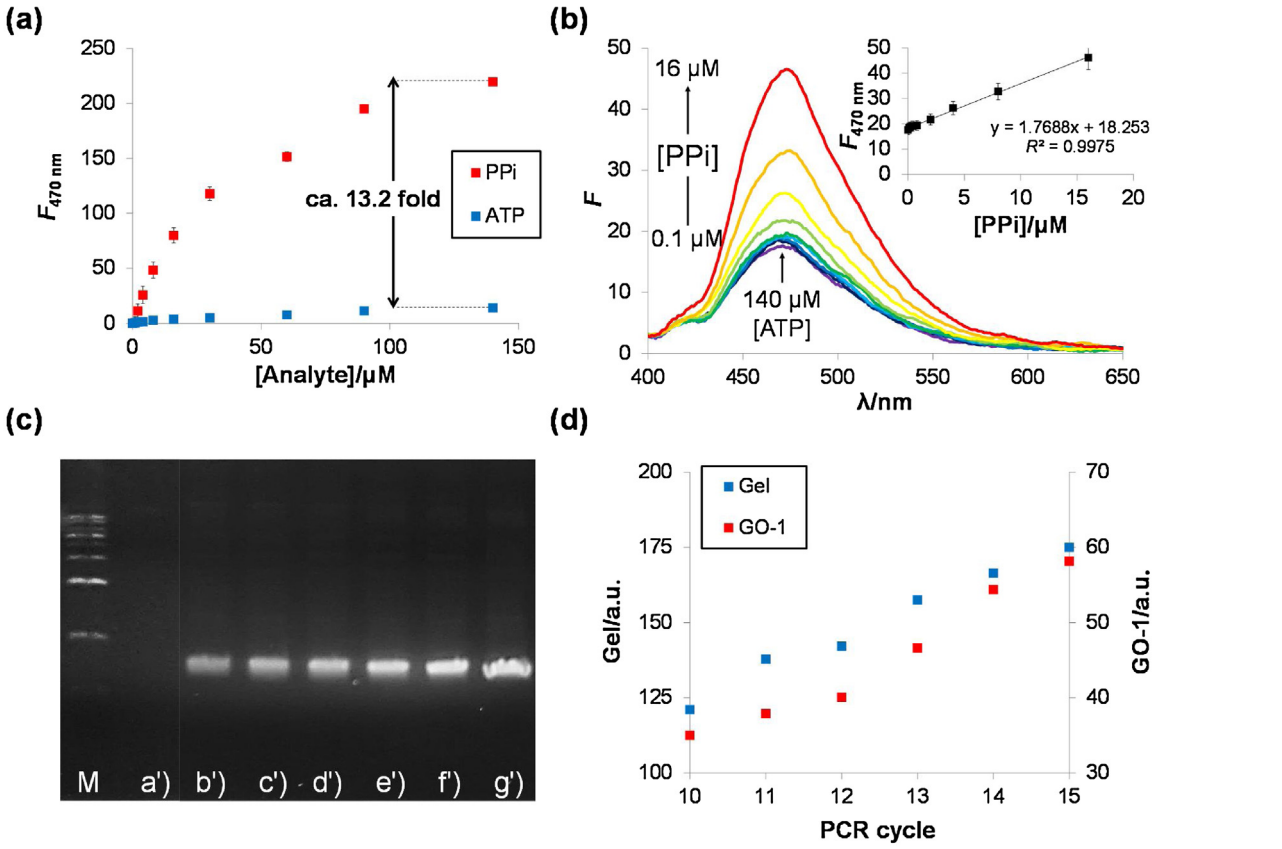

Fig. 2. (a) PPi (red square) and ATP (blue square) titration curves of GO-**1** conducted in 1 mM HEPES buffer (pH 7.4). (b) Fluorescence spectra of the GO-**1** solution against the concentration of PPi (0.1 μM–16 μM) in the co-presence of excess ATP (140 μM) in 1 mM HEPES buffer. Detection limit was determined at 2.1×10^{-6} M from 3σ/slope, where σ is the standard deviation of the fluorescence intensity in the presence of ATP (140 μM). (c) Gel electrophoresis of completed PCR mixtures. M is a standard base pair ladder. The enzymatic reaction was performed without template DNA for 15 cycles (a') and with template DNA for 10 cycles (b'), 11 cycles (c'), 12 cycles (d'), 13 cycles (e'), 14 cycles (f'), and 15 cycles (g'). (d) The DNA band intensities of gel electrophoresis (blue square) were compared with the fluorescence intensities of GO-**1** (λ_{em} = 470 nm) upon addition of the PCR product (2 μL of 10–15 cycles) in 10 mM HEPES buffer (pH 7.4) (red square). (For interpretation of the references to colour in this figure legend, the reader is referred to the web version of this article.)

is proportional to the concentration of PPi released from PCR [7]. Upon addition of the PCR product (2 μL from 10 to 15 cycles) to the GO-**1** solution, the fluorescence intensity of probe **1** (λ_{max} = 470 nm) increased linearly up to 2.9-fold relative to the negative control (PCR without template DNA), showing the same trend as the band intensity of gel electrophoresis (Fig. 2d and S15). These results indicate that GO-**1** can be used to monitor PCR in an easily accessible manner.

4. Conclusion

In conclusion, the rationally designed probe **1** readily allowed complex interplay with GO, providing an ideal model for the electrostatics-driven PPi detection method. The combination of probe **1** and GO resulted in excellent selectivity towards PPi, remarkably, even in the presence of excess ATP. Thus, GO-**1** was successfully applied for PCR monitoring. GO-**1** has potential use in real-time monitoring of enzymatic reactions in which PPi is released from NTPs. Furthermore, the sensing strategy involving GO can be applied to recognition of other anions in combination with positively-charged relevant receptors.

Acknowledgements

This work was supported by the NRF grant (Grant No. 2015R1A2A1A15055347, 2015M3A6A4076701) funded by the MSIP.

Appendix A. Supplementary data

Supplementary data associated with this article can be found, in the online version, at http://dx.doi.org/10.1016/j.snb.2017.06.018.

References

[1] M. Ronaghi, Pyrosequencing sheds light on DNA sequencing, Genome Res. 11 (2001) 3–11.
[2] L. Wang, P.G. Schultz, Expanding the genetic code, Angew. Chem. Int. Ed. 44 (2005) 34–66.
[3] S.G. Park, K.L. Ewalt, S. Kim, Functional expansion of aminoacyl-tRNA synthetases and their interacting factors: new perspectives on housekeepers, Trends Biochem. Sci. 30 (2005) 569–574.
[4] A. Trifunovic, A. Wredenberg, M. Falkenberg, J.N. Spelbrink, A.T. Rovio, C.E. Bruder, M. Bohlooly-Y, S. Gidlof, A. Oldfors, R. Wibom, J. Tornell, H.T. Jacobs, N.-G. Larsson, Premature ageing in mice expressing defective mitochondrial DNA polymerase, Nature 429 (2004) 417–423.
[5] S.G. Park, P. Schimmel, S. Kim, Aminoacyl tRNA synthetases and their connections to disease, Proc. Natl. Acad. Sci. U. S. A. 105 (2008) 11043–11049.
[6] P. Yao, P.L. Fox, Aminoacyl-tRNA synthetases in medicine and disease, EMBO Mol. Med. 5 (2013) 332–343.
[7] L.T.C. França, E. Carrilho, T.B.L. Kist, A review of DNA sequencing techniques, Q. Rev. Biophys. 35 (2002) 169–200.
[8] P.R. Schimmel, D. Söll, Aminoacyl-tRNA synthetases: general features and recognition of transfer RNAs, Annu. Rev. Biochem. 48 (1979) 601–648.
[9] K. Beebe, W. Waas, Z. Druzina, M. Guo, P. Schimmel, A universal plate format for increased throughput of assays that monitor multiple aminoacyl transfer RNA synthetase activities, Anal. Biochem. 368 (2007) 111–121.
[10] S.A. Sundberg, High-throughput and ultra-high-throughput screening: solution- and cell-based approaches, Curr. Opin. Biotechnol. 11 (2000) 47–53.

[11] Y.-W. Wu, K. Alexandrov, L. Brunsveld, Synthesis of a fluorescent analogue of geranylgeranyl pyrophosphate and its use in a high-throughput fluorometric assay for Rab geranylgeranyltransferase, Nat. Protoc. 2 (2007) 2704–2711.
[12] D.H. Lee, S.Y. Kim, J.-I. Hong, A fluorescent pyrophosphate sensor with high selectivity over ATP in water, Angew. Chem. Int. Ed. 43 (2004) 4777–4780.
[13] S.K. Kim, D.H. Lee, J.-I. Hong, J. Yoon, Chemosensors for pyrophosphate, Acc. Chem. Res. 42 (2008) 23–31.
[14] H.N. Lee, Z. Xu, S.K. Kim, K.M.K. Swamy, Y. Kim, S.-J. Kim, J. Yoon, Pyrophosphate-selective fluorescent chemosensor at physiological pH: formation of a unique excimer upon addition of pyrophosphate, J. Am. Chem. Soc. 129 (2007) 3828–3829.
[15] S. Lee, K.K.Y. Yuen, K.A. Jolliffe, J. Yoon, Fluorescent and colorimetric chemosensors for pyrophosphate, Chem. Soc. Rev. 44 (2015) 1749–1762.
[16] K.M. Kim, D.J. Oh, K.H. Ahn, Zinc(II)-dipicolylamine-functionalized polydiacetylene–liposome microarray: a selective and sensitive sensing platform for pyrophosphate ions, Chem. Asian J. 6 (2011) 122–127.
[17] W.-H. Chen, Y. Xing, Y. Pang, A highly selective pyrophosphate sensor based on ESIPT turn-on in water, Org. Lett. 13 (2011) 1362–1365.
[18] I.-S. Shin, S.W. Bae, H. Kim, J.-I. Hong, Electrogenerated chemiluminescent anion sensing: selective recognition and sensing of pyrophosphate, Anal. Chem. 82 (2010) 8259–8265.
[19] V.E. Zwicker, B.M. Long, K.A. Jolliffe, Selective sensing of pyrophosphate in physiological media using zinc(ii)dipicolylamino-functionalised peptides, Org. Biomol. Chem. 13 (2015) 7822–7829.
[20] A. Ojida, H. Nonaka, Y. Miyahara, S.-i Tamaru, K. Sada, I. Hamachi, Bis(Dpa-ZnII) appended xanthone: excitation ratiometric chemosensor for phosphate anions, Angew. Chem. Int. Ed. 45 (2006) 5518–5521.
[21] X. Peng, Y. Xu, S. Sun, Y. Wu, J. Fan, A ratiometric fluorescent sensor for phosphates: zn2+-enhanced ICT and ligand competition, Org. Biomol. Chem. 5 (2007) 226–228.
[22] C. Chung, Y.-K. Kim, D. Shin, S.-R. Ryoo, B.H. Hong, D.-H. Min, Biomedical applications of graphene and graphene oxide, Acc. Chem. Res. 46 (2013) 2211–2224.
[23] C.-H. Lu, H.-H. Yang, C.-L. Zhu, X. Chen, G.-N. Chen, A graphene platform for sensing biomolecules, Angew. Chem. Int. Ed. 48 (2009) 4785–4787.
[24] F. Wang, C. Liu, Y. Fan, Y. Wang, Z. Li, Robust detection of tyrosine phosphatase activity by coupling chymotrypsin-assisted selective peptide cleavage and a graphene oxide-based fluorescent platform, Chem. Commun. 50 (2014) 8161–8163.
[25] C. Wang, P. Yu, S. Guo, L. Mao, H. Liu, Y. Li, Graphdiyne oxide as a platform for fluorescence sensing, Chem. Commun. 52 (2016) 5629–5632.
[26] H. Zhang, S. Jia, M. Lv, J. Shi, X. Zuo, S. Su, L. Wang, W. Huang, C. Fan, Q. Huang, Size-dependent programming of the dynamic range of graphene oxide–DNA interaction-based ion sensors, Anal. Chem 86 (2014) 4047–4051.
[27] J. Balapanuru, J.-X. Yang, S. Xiao, Q. Bao, M. Jahan, L. Polavarapu, J. Wei, Q.-H. Xu, K.P. Loh, A graphene oxide–organic dye ionic complex with DNA-sensing and optical-limiting properties, Angew. Chem. Int. Ed. 49 (2010) 6549–6553.
[28] Y. Xu, A. Malkovskiy, Y. Pang, A graphene binding-promoted fluorescence enhancement for bovine serum albumin recognition, Chem. Commun. 47 (2011) 6662–6664.
[29] X. Gu, G. Yang, G. Zhang, D. Zhang, D. Zhu, A new fluorescence turn-on assay for trypsin and inhibitor screening based on graphene oxide, ACS Appl. Mater. Interfaces 3 (2011) 1175–1179.
[30] W. Lin, L. Yuan, Z. Cao, Y. Feng, J. Song, Through-bond energy transfer cassettes with minimal spectral overlap between the donor emission and acceptor absorption: coumarin–rhodamine dyads with large pseudo-stokes shifts and emission shifts, Angew. Chem. Int. Ed 49 (2010) 375–379.
[31] H.-W. Rhee, S.H. Lee, I.-S. Shin, S.J. Choi, H.H. Park, K. Han, T.H. Park, J.-I. Hong, Detection of kinase activity using versatile fluorescence quencher probes, Angew. Chem. Int. Ed. 49 (2010) 4919–4923.
[32] D. Yang, A. Velamakanni, G. Bozoklu, S. Park, M. Stoller, R.D. Piner, S. Stankovich, I. Jung, D.A. Field, C.A. Ventrice Jr, R.S. Ruoff, Chemical analysis of graphene oxide films after heat and chemical treatments by X-ray photoelectron and Micro-Raman spectroscopy, Carbon 47 (2009) 145–152.
[33] Z. Fan, K. Wang, T. Wei, J. Yan, L. Song, B. Shao, An environmentally friendly and efficient route for the reduction of graphene oxide by aluminum powder, Carbon 48 (2010) 1686–1689.
[34] A.V. Murugan, T. Muraliganth, A. Manthiram, Rapid, facile microwave-solvothermal synthesis of graphene nanosheets and their polyaniline nanocomposites for energy strorage, Chem. Mater. 21 (2009) 5004–5006.
[35] M.C. Biesinger, L.W.M. Lau, A.R. Gerson, R.S.C. Smart, Resolving surface chemical states in XPS analysis of first row transition metals, oxides and hydroxides: Sc Ti, V, Cu and Zn, Appl. Surf. Sci. 257 (2010) 887–898.
[36] M. Wu, R. Kempaiah, P.-J.J. Huang, V. Maheshwari, J. Liu, Adsorption and desorption of DNA on graphene oxide studied by fluorescently labeled oligonucleotides, Langmuir 27 (2011) 2731–2738.
[37] Y. Li, Y. Duan, J. Zheng, J. Li, W. Zhao, S. Yang, R. Yang, Self-assembly of graphene oxide with a silyl-appended spiropyran dye for rapid and sensitive colorimetric detection of fluoride ions, Anal. Chem. 85 (2013) 11456–11463.
[38] Q. Su, S. Pang, V. Alijani, C. Li, X. Feng, K. Müllen, Composites of graphene with large aromatic molecules, Adv. Mater. 21 (2009) 3191–3195.
[39] GO-1 conjugate is stable enough to test all the experiments for at least 2 weeks.
[40] Y. Hu, T. Guo, X. Ye, Q. Li, M. Guo, H. Liu, Z. Wu, Dye adsorption by resins: effect of ionic strength on hydrophobic and electrostatic interactions, Chem. Eng. J. 228 (2013) 392–397.
[41] A. Kasry, A.A. Ardakani, G.S. Tulevski, B. Menges, M. Copel, L. Vyklicky, Highly efficient fluorescence quenching with graphene, J. Phys. Chem. C 116 (2012) 2858–2862.

Biographies

Dong-Nam Lee received his B.S. (2008) and M.S. (2010) degree in Chemistry at Kyonggi University, and Ph.D. degree (2017) in Organic Chemistry at Seoul National University. He is continuing his postdoctoral studies at Seoul National University under the direction of Professor Jong-In Hong in the area of Bioorganic Chemistry. His current research interest focuses on exploiting the electronic effect for the development of innovative sensing systems for selective detection of biologically important targets.

Jungwon Kim obtained his M.S. degree in biochemistry from Chung-Ang University in 2015. Now he is a researcher at an institute of Biomedical Engineering in Kyunghee University, Korea. His research interests are focused on the synthesis of functional polymer materials and their applications in bio-electrochemical analysis.

Jae Gyu Jang is enrolled in MS/Ph.D. program in the Department of Chemistry, Seoul National University, Korea. His research interest includes the development of supramolecular superstructures with carbon materials and organic small molecules.

Jong-In Hong received his Ph.D. in Chemistry from Columbia University in 1990 with Prof. W. Clark Still. After postdoctoral studies with Prof. Julius Rebek, Jr. at M.I.T. (1991–1992), he joined Seoul National University in 1993 as an Assistant Professor, and became a Professor in 2004. His research interests include molecular recognition and sensing of biologically significant compounds and the development of organic functional materials such organic light-emitting diodes and organic solar cells.